

Supporting Information

A Benzothiadiazole-Decorated UiO-68 Metal-Organic Framework for Diclofenac and Ibuprofen Luminescence Sensing and Adsorption in Wastewater

*Giacomo Provinciali,^a Giulio Bicchierai,^a Agostina Lina Capodilupo,^b Anna Mauri,^c Jia Fu,^d Dahuan Liu^{*d} Giuliano Giambastiani,^{e,f,a} Giulia Tuci,^{a,f} Simona Galli,^{*c,f} Clara Piccirillo,^{*b} and Andrea Rossin^{*a,f}*

^a Istituto di Chimica dei Composti Organometallici (CNR-ICCOM), Via Madonna del Piano 10, Sesto Fiorentino (Firenze), 50019, Italy. E-mail: a.rossin@iccom.cnr.it

^b CNR NANOTEC, Istituto di Nanotecnologia, Campus Ecoteckne, Via Monteroni, 73100 Lecce, Italy. E-mail: clara.piccirillo@nanotec.cnr.it

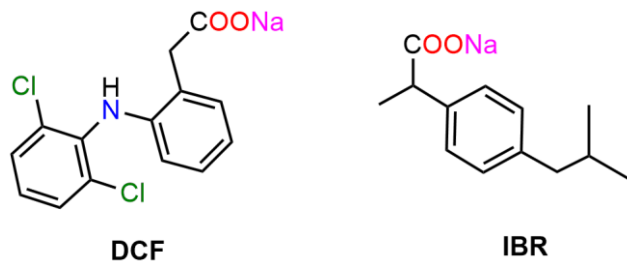
^c Dipartimento di Scienza e Alta Tecnologia, Università degli Studi dell’Insubria, Via Valleggio 11, 22100 Como, Italy. E-mail: simona.galli@uninsubria.it

^d State Key Laboratory of Organic-Inorganic Composites, Beijing University of Chemical Technology, Beijing 100029, China. E-mail: liudh@mail.buct.edu.cn

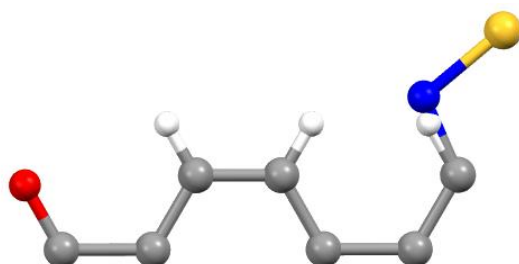
^e Dipartimento di Chimica Ugo Schiff, Università di Firenze, Via della Lastruccia 3-13, 50019 Sesto Fiorentino (Firenze), Italy.

^f Consorzio Interuniversitario Nazionale per la Scienza e Tecnologia dei Materiali (INSTM), Via G. Giusti, 9 50121 Firenze, Italy.

Supporting Information



Scheme S1. Molecular structure of the water pollutants examined in this study: Diclofenac Sodium (DCF) and Ibuprofen Sodium (IBR).



Scheme S2. Molecular structure of the rigid body adopted to concomitantly model the two linkers. Element colour code: carbon, grey; hydrogen, white; nitrogen, blue; oxygen, red; sulphur, yellow.

Supporting Information

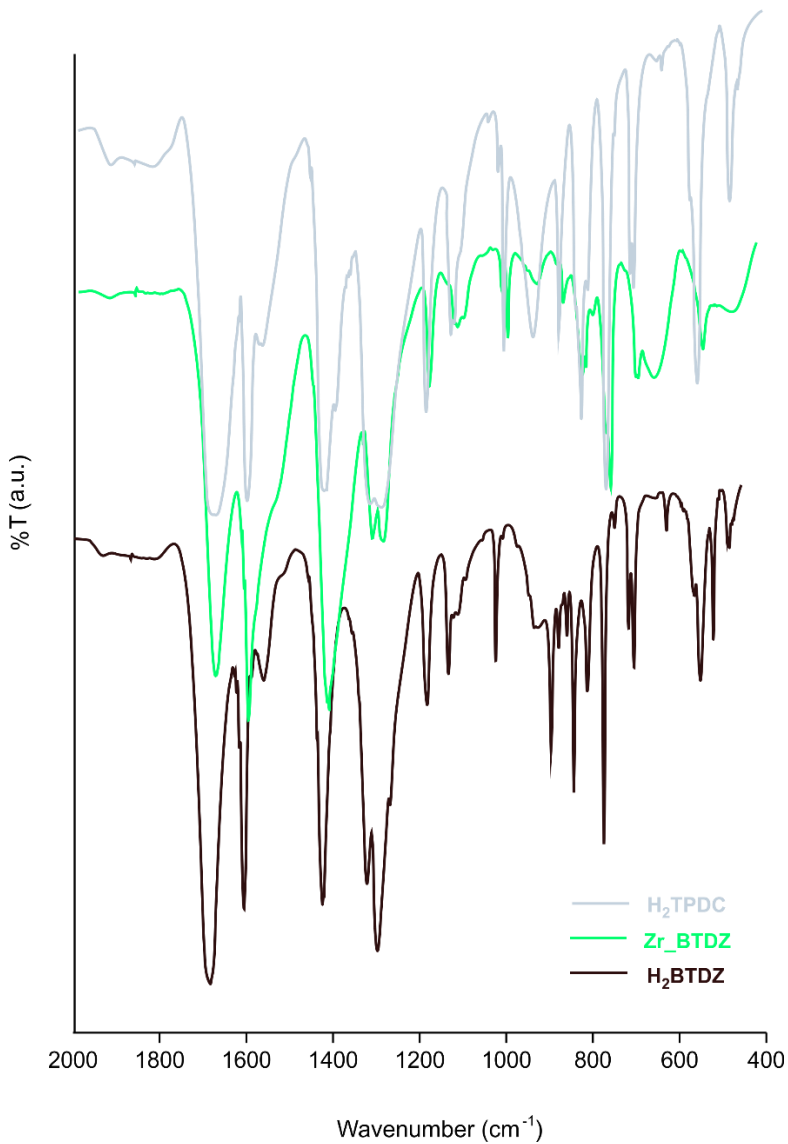


Figure S1. Infrared spectra (KBr, T = 298 K, 2000-400 cm^{-1}) of **Zr_BTDZ** and its constitutive linkers H₂TPDC and H₂BTDZ at comparison.

Supporting Information

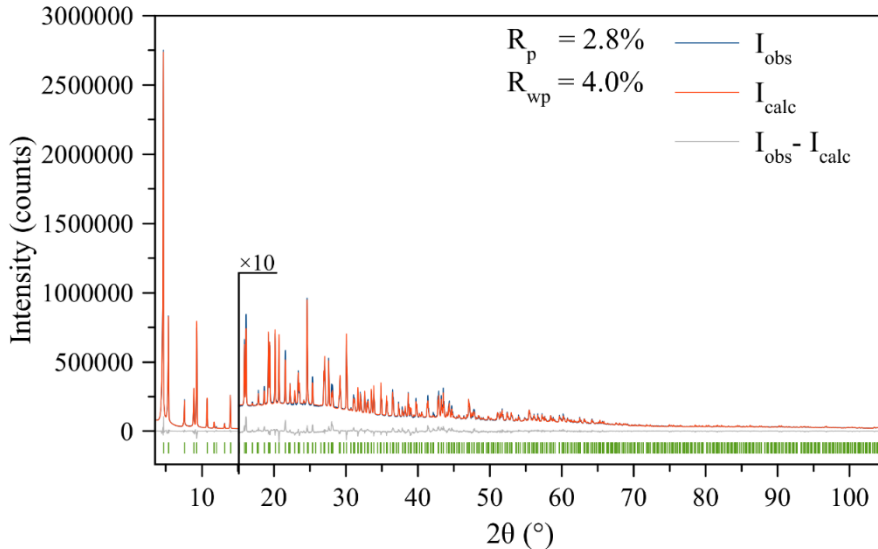


Figure S2. Graphical representation of the final stage of the structure refinement, carried out with the Rietveld method, on the powder X-ray diffraction data of a sample of thermally activated **Zr_BTDZ**. Observed, calculated and difference patterns: blue, red and grey trace, respectively. The green ticks above the horizontal axis indicate the positions of the Bragg reflection maxima. The portion above 15° has been magnified for the sake of visibility.

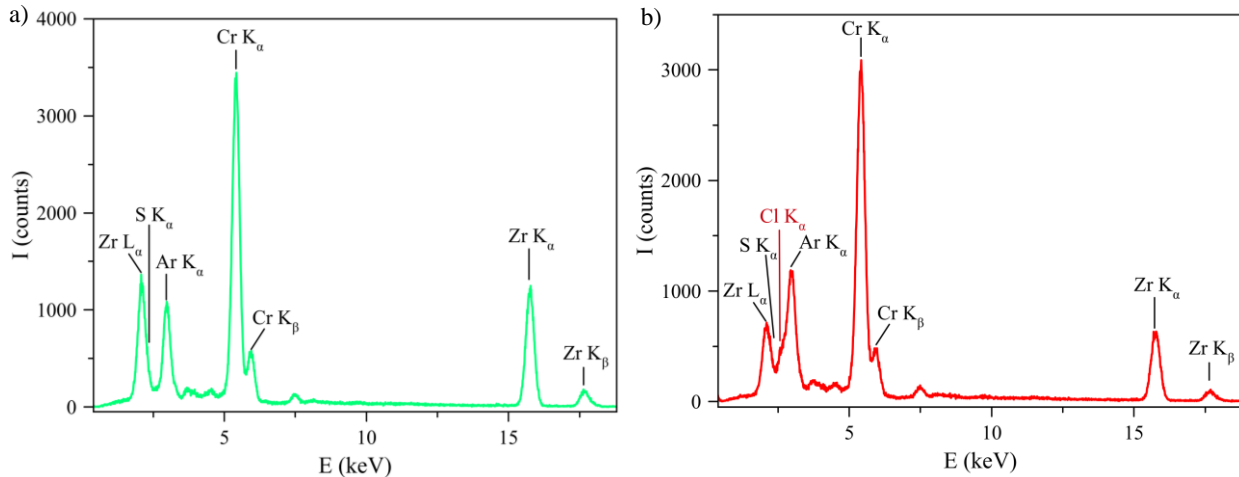


Figure S3. X-ray fluorescence spectra of powdered samples of (a) thermally activated **Zr_BTDZ** and (b) **[DCF@Zr_BTDZ]**, with the corresponding elemental analysis. The signals of chromium are due to the chemical nature of the X-ray source anode, while the signal of argon descends from the fact that the spectra were acquired in air.

Supporting Information

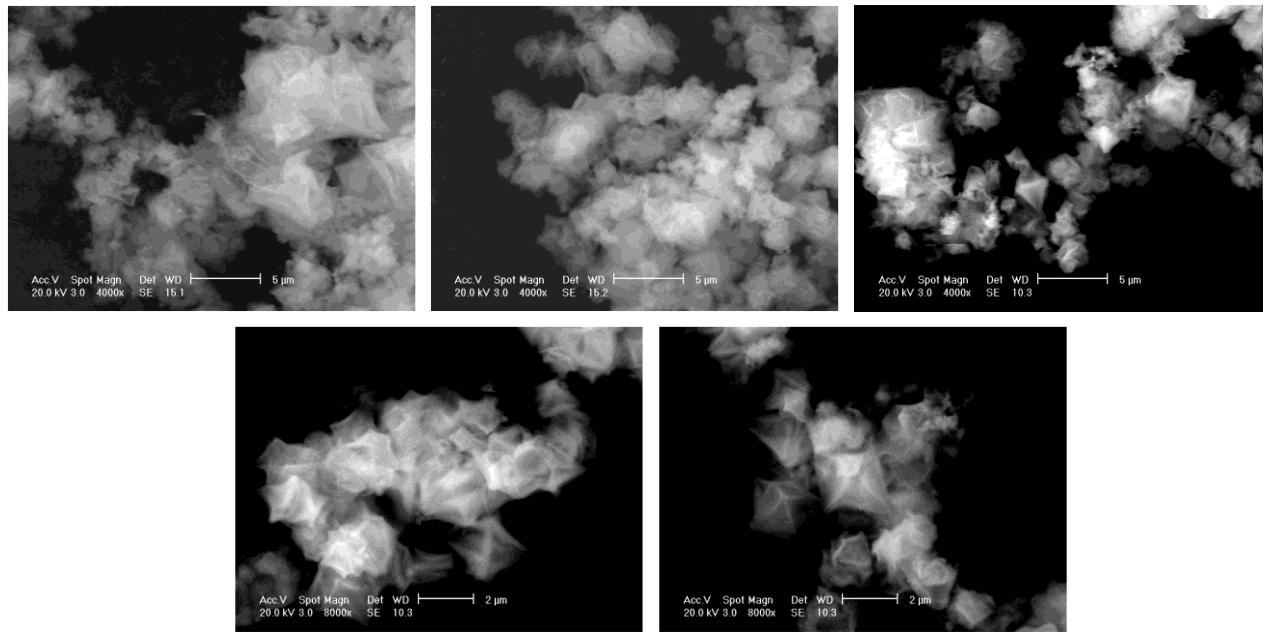


Figure S4. Scanning electron microscopy images of a powdered sample of **Zr_BTDZ**.

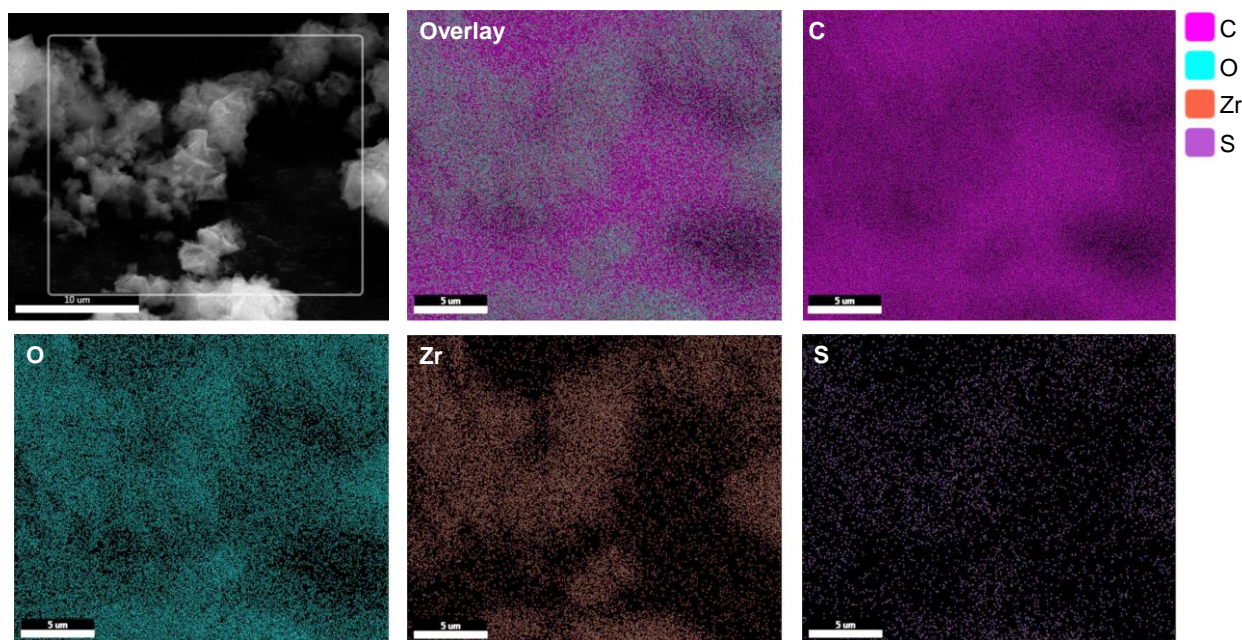


Figure S5. Energy dispersive X-ray analysis of **Zr_BTDZ** employed for the acquisition of the images in collected in Figure S4. The distribution of carbon (also due to the carbon tape on which the sample was deposited), oxygen, zirconium and sulphur can be appreciated.

Supporting Information

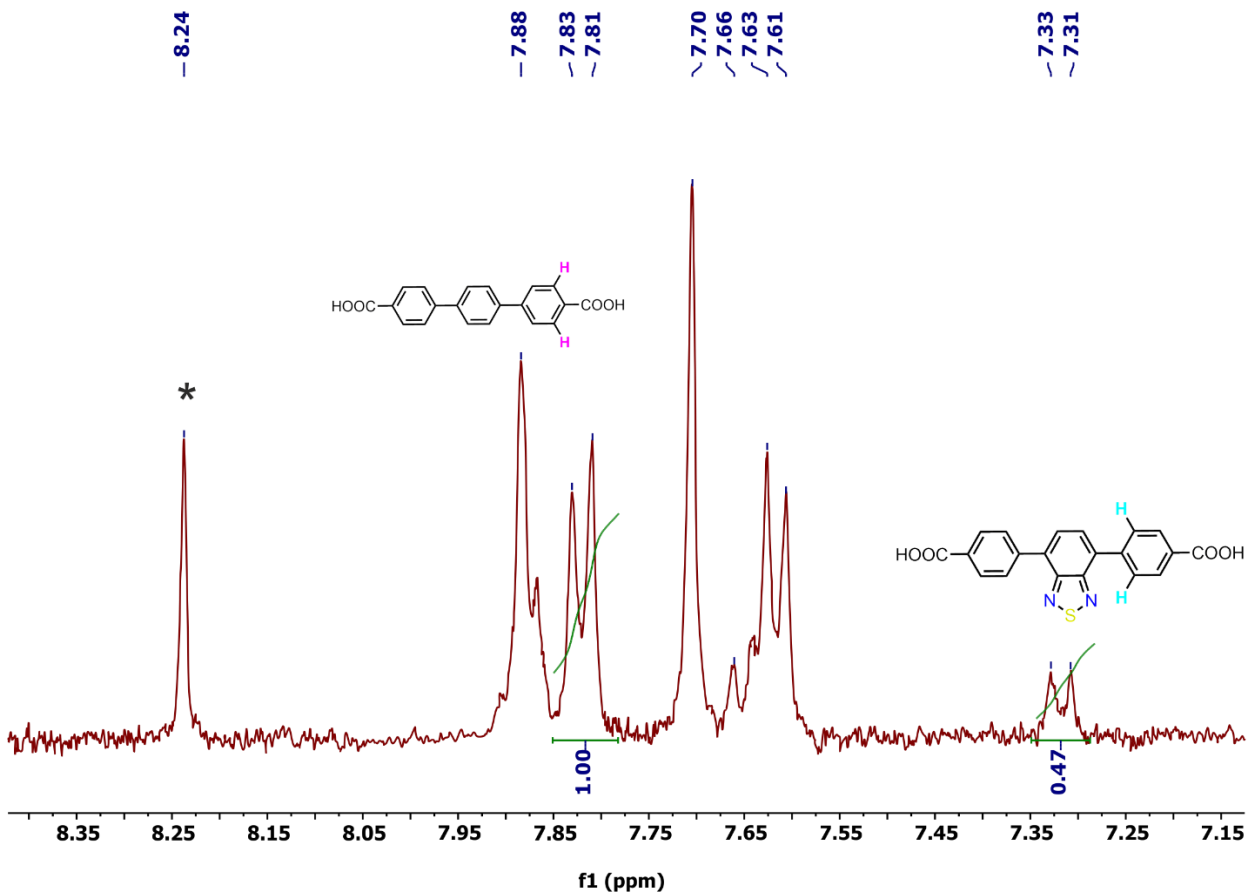


Figure S6. ^1H NMR spectrum [400 MHz, Na(OD)/D₂O/DMSO- d_6 , 298 K] of digested Zr_BTDZ·DMF. Highlighted the signals of the two ligands used to retrieve their stoichiometric ratio. The asterisk marks a signal of DMF.

Supporting Information

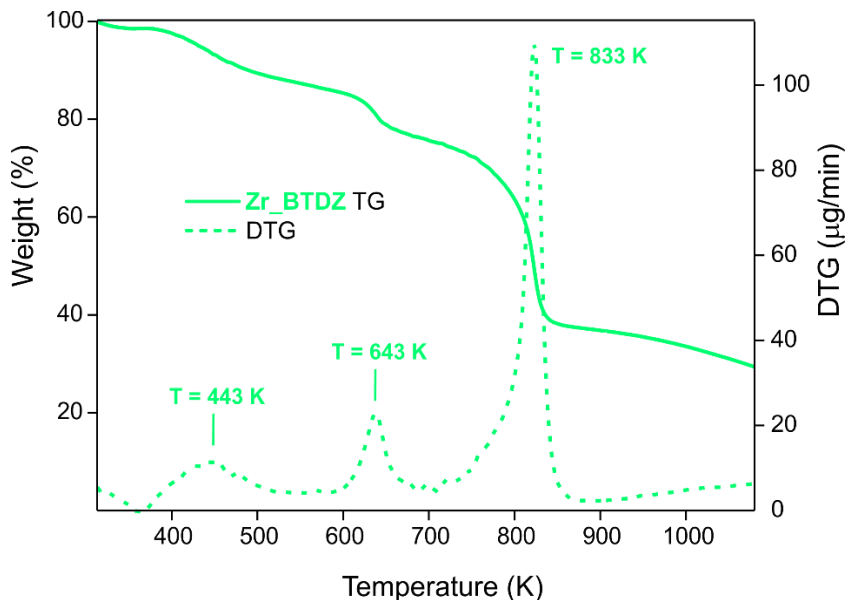


Figure S7. TG-DTG traces of **Zr_BTDZ**.

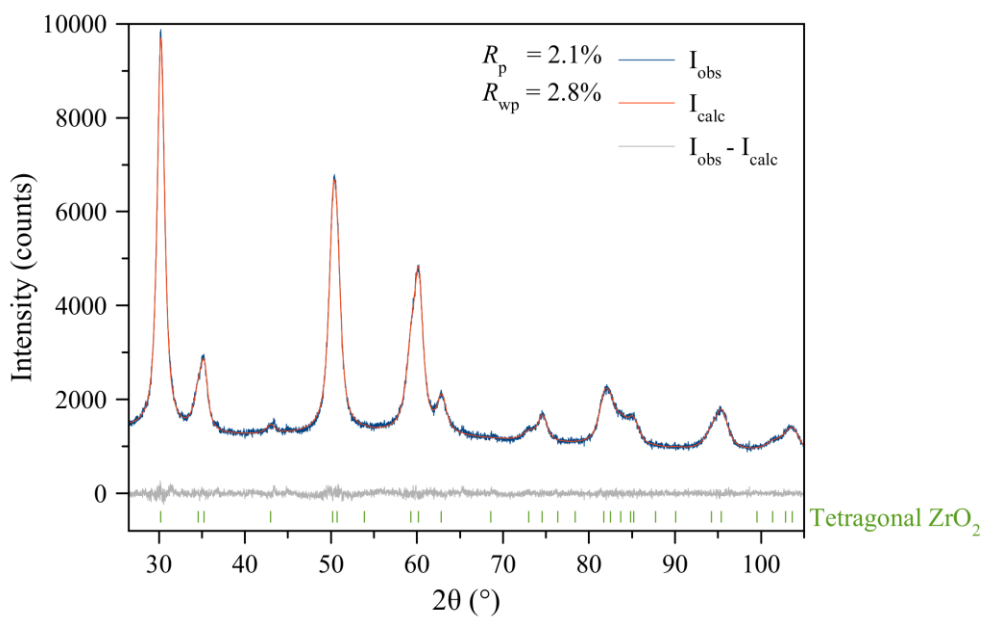


Figure S8. Whole powder pattern refinement carried out with the Le Bail method on the powder X-ray diffraction pattern of the solid residue recovered at the end of the thermal analysis performed on **Zr_BTDZ** with the space group and unit cell parameters of the tetragonal polymorph of ZrO_2 (ICSD entry 68589). Observed, calculated and difference patterns: blue, red and grey trace, respectively. The green ticks above the horizontal axis indicate the positions of the Bragg reflection maxima of tetragonal ZrO_2 .

Supporting Information

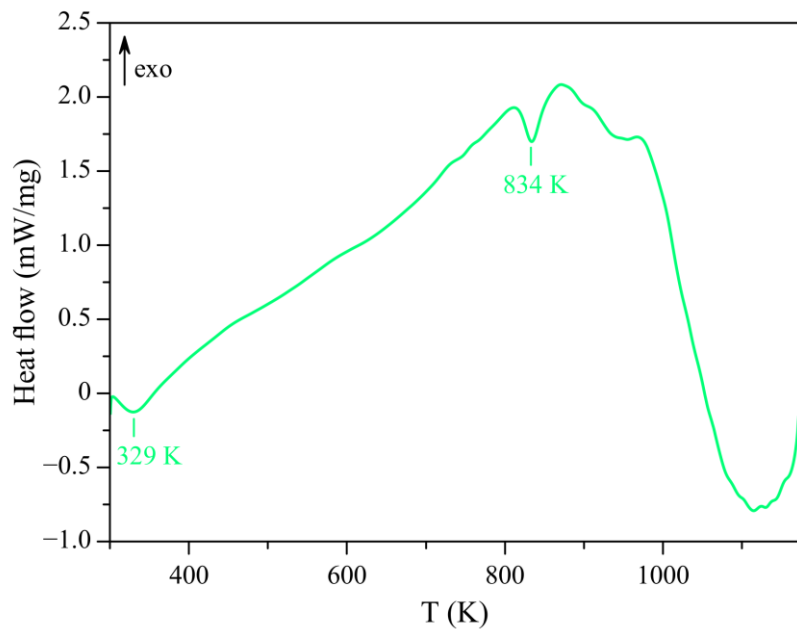


Figure S9. DSC trace of thermally activated **Zr_BTDZ**.

Supporting Information

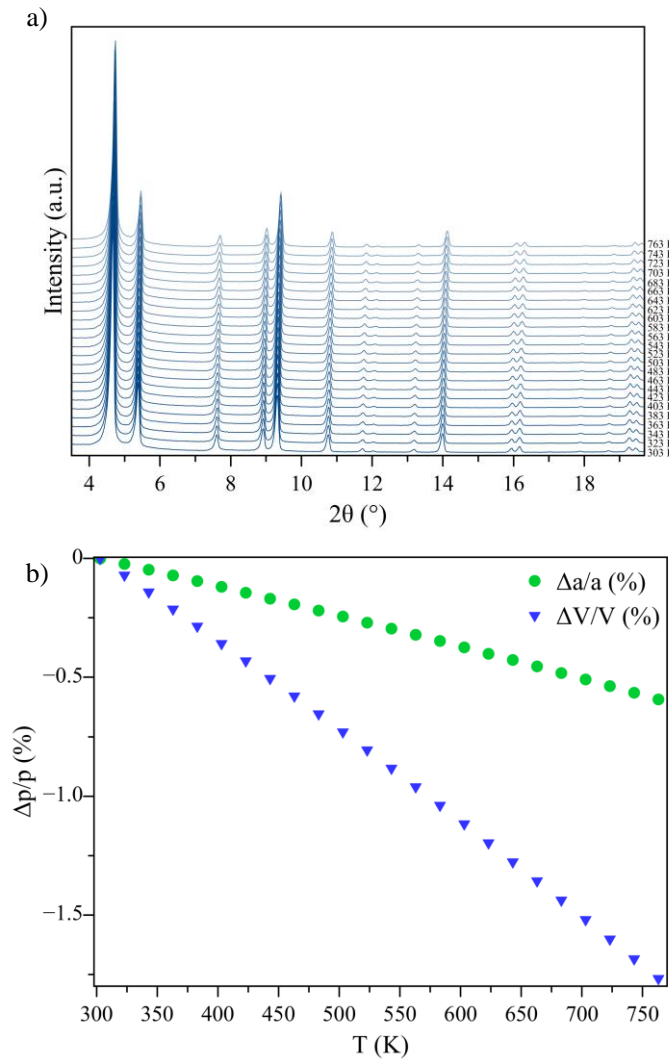


Figure S10. (a) Temperature-resolved powder X-ray diffraction patterns acquired in air on a sample of thermally activated **Zr_BTDZ** in the temperature range 303-763 K. (b) Percentage relative variation of the unit cell parameters (p) of **Zr_BTDZ** as a function of the temperature, retrieved by means of a parametric whole powder pattern refinement on the data shown in (a).

Supporting Information

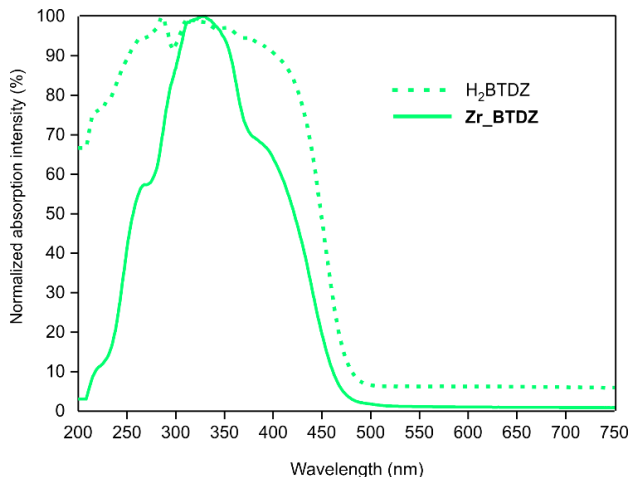


Figure S11. Absorption spectra of H₂BTDZ and Zr_BTDZ at comparison.

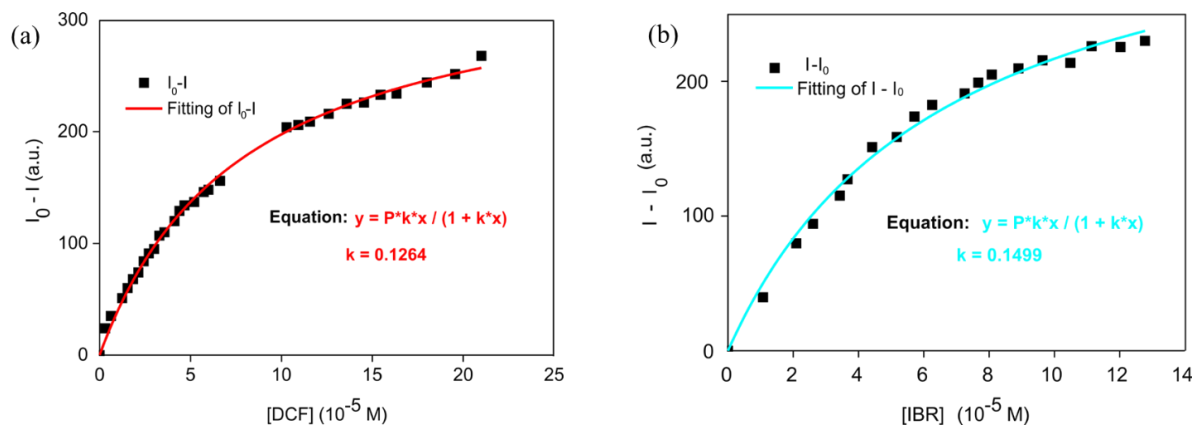


Figure S12. Benesi-Hildebrand fitting on the ΔI vs. [C] plots for the determination of the K_b values of DCF and IBR for Zr_BTDZ.

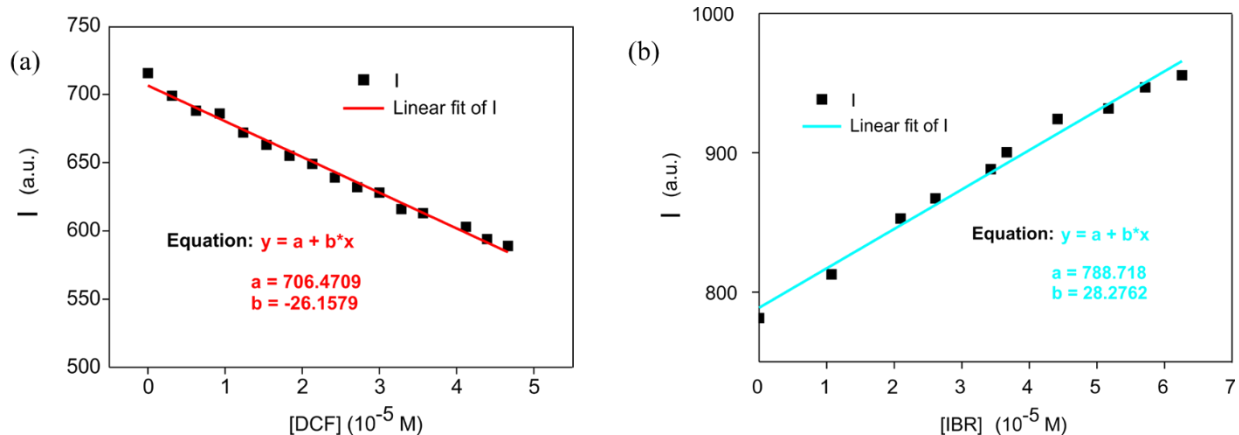


Figure S13. Linear fitting on the I vs. [C] plots for the determination of the LOD values of DCF and IBR by Zr_BTDZ.

Supporting Information

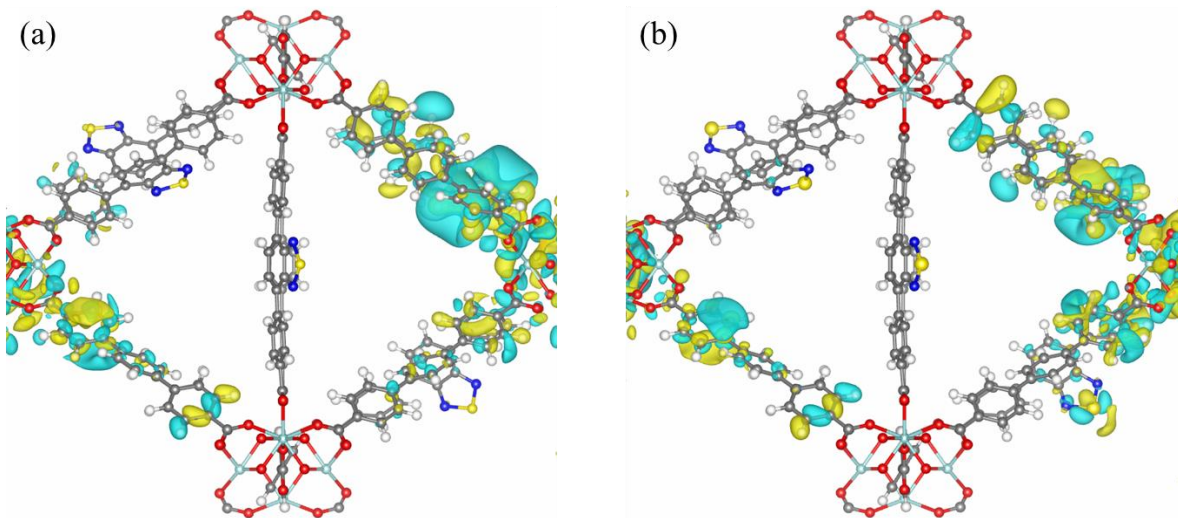


Figure S14. (a) HOCO and (b) LUCO of **Zr_BTDZ**.

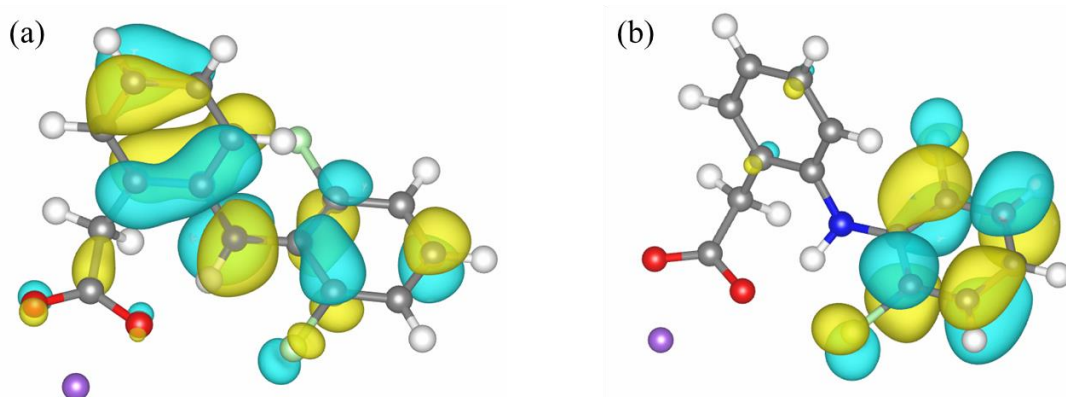


Figure S15. (a) HOMO ($E = -4.001135$ eV) and (b) LUMO ($E = -0.706570$ eV) of DCF.

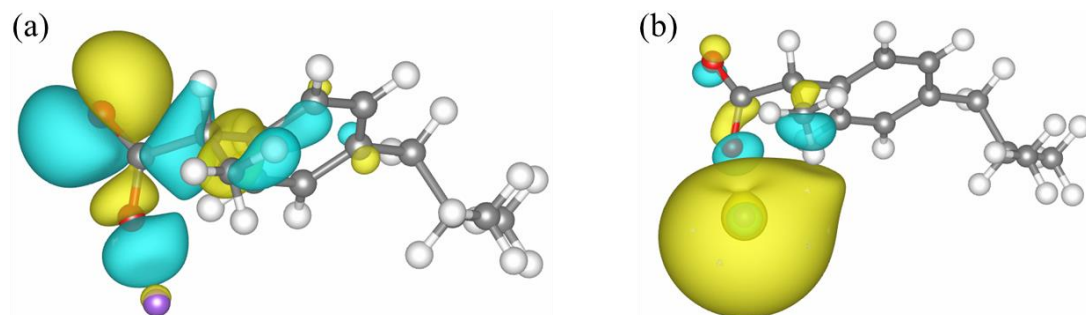


Figure S16. (a) HOMO ($E = -3.799980$ eV) and (b) LUMO ($E = -1.040722$ eV) of IBR.

Supporting Information

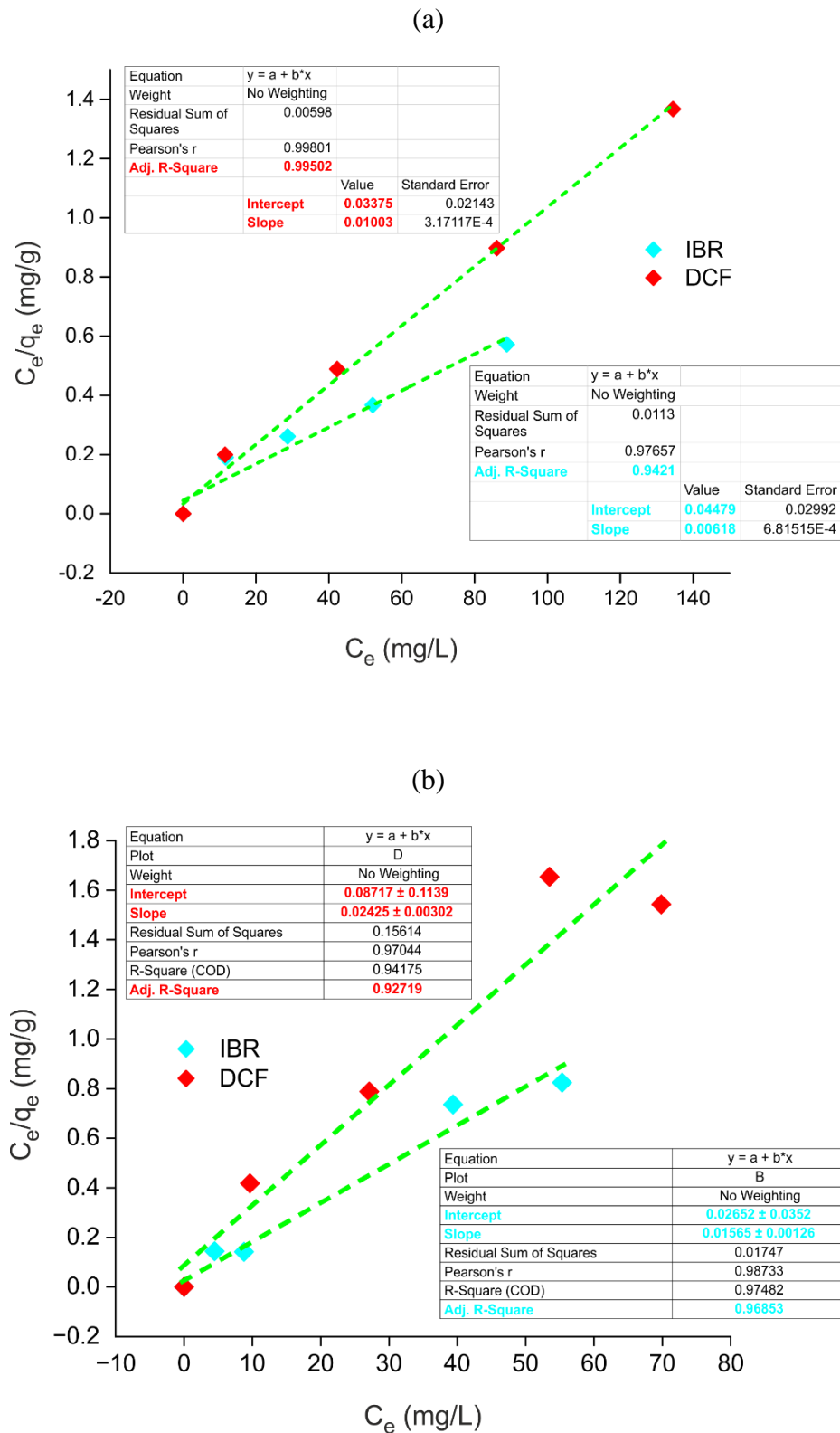


Figure S17. Adsorption data on the (a) single-component and (b) binary mixture fitting on Zr_BTDZ according to a Langmuir model.

Supporting Information

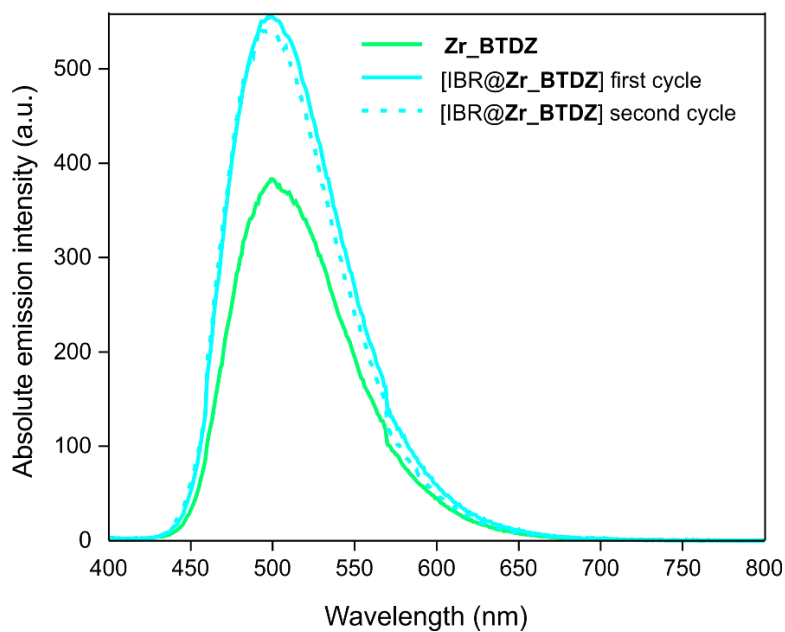


Figure S18. Luminescence spectra acquired for **Zr_BTDZ** after two successive IBR adsorption and desorption cycles.

Supporting Information

Table S1. Comparison of the DCF/IBR adsorption performance of **Zr_BTDZ** with other Zr^{IV} MOFs from the literature.

MOF	SSA [m ² /g]	X _m (DCF) [mg/g]	X _m (IBR) [mg/g]	Reference
Zr_BTDZ	3770	100	161.3	This work
TTz@PCN-700	757	263	---	[1]
TzPhTz ^{Me} @PCN-700	547	167	---	[1]
UiO-67-TzTz	1310	62	---	[2]
PCN-134	756	649	---	[3]
MOF-525	427	519	---	[4]
UiO-66	1082/1123	189	127	[5/6]
UiO-66-NH ₂	902/532	106	55	[7/8]
Zr-MOF- NH ₂ /triptophane	730	---	371	[9]
UiO-67-BA(10)	2900	---	213	[10]
UiO-66-SO ₃ H	910	263		[7]
UiO-66-(COOH) ₂	980	480		[11]
MOF-808	1517/1314	833	300	[12/13]
MOF-802	5	---	48	[13]
ZJU-101	561	546		[14]

Supporting Information

References

1. G. Provinciali, A. L. Capodilupo, A. Mauri, S. Galli, L. Donà, B. Civalleri, G. Tuci, G. Giambastiani, C. Piccirillo and A. Rossin, *ACS ES&T Water*, 2024, **4**, 2339-2351
2. G. Mercuri, M. Moroni, S. Galli, C. Piccirillo, A. Capodilupo, G. Tuci, G. Giambastiani and A. Rossin, *Inorg. Chem. Front.*, 2022, **9**, 90-102
3. Y. Gao, J. Xia, D. Liu, R. Kang, G. Yu and S. Deng, *Chem. Eng. J.*, 2019, **378**, 122118
4. F. Zhao, S. Fang, Y. Gao and J. Bi, *J. Colloid Interf. Sci.*, 2022, **615**, 876-886
5. Z. Hasan, N. Abedin Khan and S. H. Jhung, *Chem. Eng. J.*, 2016, **284**, 1406-1413
6. C. Cretu, R. Nicola, S.-A. Marinescu, E.-M. Picioruș, M. Suba, C. Duda-Seiman, A. Len, L. Illés, Z. E. Horváth and A.-M. Putz, *Int. J. Mol. Sci.*, 2023, **24**, 13887
7. S. Zhuang, R. Cheng and J. Wang, *Chem. Eng. J.*, 2019, **359**, 354-362
8. H.-L. Wang, H. Yeh, B.-H. Li, C.-H. Lin, T.-C. Hsiao and D.-H. Tsai, *ACS Appl. Nano Mater.*, 2019, **2**, 3329-3334
9. N. D. Alkhathami, N. A. Alamrani, A. Hameed, S. D. Al-Qahtani, R. Shah and N. M. El-Metwaly, *Polyhedron*, 2023, **235**, 116349
10. M. M. H. Mondol, D. K. Yoo and S. H. Jhung, *J. Environ. Chem. Eng.*, 2022, **10**, 108560
11. H. A. Younes, M. Taha, R. Mahmoud, H. M. Mahmoud and R. M. Abdelhameed, *J. Colloid Interf. Sci.*, 2022, **607**, 334-346
12. N. Prasetya and K. Li, *Chem. Eng. J.*, 2021, **417**, 129216
13. S. Lin, Y. Zhao and Y.-S. Yun, *ACS Appl. Mater. Interfaces*, 2018, **10**, 28076-28085
14. Y. Yang, Q. Hu, Q. Zhang, K. Jiang, W. Lin, Y. Yang, Y. Cui and G. Qian, *Mol. Pharmaceutics*, 2016, **13**, 2782-2786